Supporting Information

Evaluating nonideality in binary mbCD/Sucrose solutions. Nonideality in dilute mbCD/Sucrose solutions arises from i) large molecular sizes of both solutes and ii) solute-solute interactions between mbCD and Sucrose. Contributions from solute-solute interactions were accounted for by determining the difference between measured osmolarities and calculated osmolarities assuming no solute-solute interactions. Quantitatively, this difference is given by:

$$\text{Eq. S1: } \Delta\text{Osm}_{\text{mbCD - Sucr}} = \text{Osm}_{\text{measured}} - i_{\text{mbCD}}[\text{mbCD}] - i_{\text{Sucr}}[\text{Sucrose}]$$

where $Osm_{measured}$ is the measured osmolarity of a mbCD/Sucrose solution; $[\text{mbCD}]$ and $[\text{Sucrose}]$ are the total concentrations of mbCD and Sucrose, respectively, in a solution; and i_{mbCD} and i_{Sucr} are the osmotic coefficients of mbCD and Sucrose, respectively, determined in the absence of the other solute. It was determined that $i_{\text{mbCD}} = 1.15$ and $i_{\text{Sucr}} = 1.13$. Summaries of $\Delta\text{Osm}_{\text{mbCD - Sucr}}$ for different mbCD/Sucrose solutions are shown in Figures S1a and S1b; from these, it shows that binary mbCD/Sucrose solutions are more hypertonic than naïvely expected, indicating nonideal behavior. $\Delta\text{Osm}_{\text{mbCD - Sucr}}$ was second order with respect to $[Sucrose]$ (see Figure S1a) and first-order with respect to $[\text{mbCD}]$ (see Figure S1b). In Figure S1a, each series of increasing $[\text{mbCD}]$ was fit to a 2nd-order polynomial with respect to $[\text{Sucrose}]$ with the intercept set to zero; in Figure S1b, each series of increasing $[\text{Sucrose}]$ was fit to a linear equation with respect to $[\text{mbCD}]$ with the intercept set to zero. The fitting was performed via polynomial regression using the Solver add-on in Microsoft Excel. Data in Figures S1c and S1d were obtained from each of these fittings. By fitting data in Figures S1c and S1d, the following empirical fit for $\Delta\text{Osm}_{\text{mbCD - Sucr}}$ was obtained:

$$\text{Eq. S2: } \Delta\text{Osm}_{\text{mbCD - Sucr}} = C_A[\text{mbCD}][\text{Sucrose}]^2$$

where C_A is an empirical fitting parameter with a value of $(1.74 \pm 0.05) \times 10^{-5}$ mOsm L^{-1} mM^{-3} (value ± uncertainty from fitting).

Empirical fitting showed that nonideality in binary mbCD/Sucrose solutions depended first-order on $[\text{mbCD}]$ and second-order on $[\text{Sucrose}]$. These dependences suggested that mbCD and Sucrose form aqueous phase complexes with a stoichiometry of 1:2, respectively. Therefore, data in Figure S1a and S1b were also fit to an equilibrium binding model in which the stoichiometries were fixed to these estimates; this was again accomplished by regression using the Solver add-on in Microsoft Excel. The equilibrium constant, $K_{\text{mbCD - Sucr}}$, for this interaction is given by:

$$\text{Eq. S3: } K_{\text{mbCD - Sucr}} = \frac{[\text{mbCD - Sucr}_2]}{[\text{mbCD}]_{\text{free}}[\text{Sucrose}]_{\text{free}}^2}$$

where $[\text{mbCD - Sucr}_2]$ is the equilibrium concentration of complex formed between a single mbCD molecule and two Sucrose molecules; $[\text{mbCD}]_{\text{free}}$ and $[\text{Sucrose}]_{\text{free}}$ are the equilibrium concentrations of unbound mbCD and Sucrose, respectively. From this fitting, it was determined that $K_{\text{mbCD - Sucr}} = 8163$ M^{-1} and an osmotic coefficient of $i_{\text{mbCD - Sucr}} = 5.5$. Residuals with respect to

$[\text{Sucrose}]$ and $[\text{mbCD}]$ for the empirical fitting (orange squares) and fitting to the equilibrium binding model (blue circles) are shown in Figures S1e and S1f, respectively.

These measurements show that binary mbCD/Sucrose solutions behave nonideally and that this originates from solute-solute interactions. Restated, this means that a binary mbCD/Sucrose solution is slightly more hypertonic than a solution containing only one of these solutes with a molarity matching the summed molarities of mbCD/Sucrose in the former. Because of the nonlinearity of the fits, it was difficult to precisely account for nonideality (refer to the residuals in Figures S1e and S1f); attempting to do so introduced variable osmotic-swelling/deflation of vesicles within single experimental series, thereby confounding our interpretation of experiments. To bypass this, the more straightforward approach in which the mbCD/Sucrose concentrations were simultaneously adjusted in the external solution such that all vesicles (which encapsulated Sucrose only) ubiquitously experienced hypertonic differentials (which nonetheless approached isotonicity compared to earlier studies on the complexation behavior of mbCD with lipid)[1-3].

To account for this nonideal behavior in GUV experiments, a practical threshold for osmotic deflation was devised (that is, no more than 2% deflation of GUVs encapsulated with 150 mM Sucrose) and was not exceeded. This corresponded to a deviation of no more than +5 mOsm/L from nonideality, associated with mbCD/Sucrose concentrations of 25 mM and 125 mM, respectively. These concentrations were not exceeded in any of the GUV experiments throughout the associated study (refer to main text).

Characterization of GUV dispersions used in the associated study. GUVs yielded by electroformation are known to display a variety of high-curvature protrusions[4] and are reflective of area asymmetry remaining within them[5, 6]. This residual area asymmetry can be relaxed by lipid flip-flop (which is accelerated by elevated temperature).[7] As such, every GUV dispersion was annealed at 50 ^{o}C overnight to abrogate this asymmetry via acceleration of lipid flip-flop; this was followed by measurement of the total lipid concentration in every dispersion via mass spectrometry (refer to Materials and Methods in main text); see Table S1. From mass spectrometric quantification, the POPC concentration in these dispersions was $[\text{POPC}]_{\text{GUVs}} = 44 \pm 4\ \mu\text{M}$ (average ± SEM; from eleven GUV dispersions). The effectiveness of this approach was assessed by measuring changes in the accessibility of NBD-PE via fluorescence quenching (refer to Materials and Methods in main text) (Figure S2b) and by morphological evaluation of three GUV dispersions before/after annealing (refer to Materials and Methods in main text) (Figures S2c/S2d). Prior to annealing, GUVs contained extensive area asymmetry (with more lipid in their outer leaflets, on average), indicated by the high frequency of GUVs with outward bending protrusions. After annealing, the area asymmetry was reduced (leading to a more uniform lipid distribution between their leaflets, on average), indicated by the decrease in the NBD-PE lipid accessibility, decrease in the frequency of GUVs with outward bending protrusions, and also by the increase in GUVs containing no bending protrusions.

Investigating the re-nucleation behavior of complex solutions induced by dilution. Having investigated the re-nucleation behavior of loaded mbCD solutions by thermal cycling, we also studied another means by which re-nucleation can be induced: that is, dilution at a fixed temperature (as performed earlier)[2]. In a previous study, solutions in the solubilization region were diluted whereupon re-nucleation occurred. Eq. 6 in the main text predicts that the act of dilution

simultaneously adjusts $[\mathrm{mbCD}]_{\mathrm{total}}$ and $[\mathrm{POPC}]_{\mathrm{total}}$, causing an instantaneous increase in Q_ϕ equivalent to the dilution-factor raised to the third-power (following from the 1:4 lipid:mbCD stoichiometry of the complexes; see Eq. 1 in the man text). This can be used to map initial/final values of Q_ϕ before/after dilution onto the phase diagram, yielding a trajectory that is spanned during this process. Extending this calculation to the previous study[2] yields the trajectory labelled as "1" in Figure S3a which crosses the solubilization boundary. This suggests that re-nucleation in response to dilution occurs only if dilution promotes the mixture to the coexistence region. To confirm this hypothesis (i.e. to see if re-nucleation was path-dependent), we diluted a complex solution at 25 °C (under continuous stirring; 400 RPM) such that the undiluted/diluted states remained in the solubilization region (see the trajectory labelled as "2." in Figure S3a). We detected no re-nucleation through this trajectory, confirming the above hypothesis (i.e. re-nucleation was path-independent). This means that re-nucleation from dilution obeys the RT phase diagram, as determined by light scattering titrations (Figure 1c). Restated through mass-action, this implies that re-nucleation occurs only if the instantaneous value of Q_ϕ immediately after dilution satisfies $Q_\phi > 214\ \mathrm{M}^{-3}$ (I.e. the value of K_{eff} at the RT solubilization boundary). If this is valid, then the equilibrium condition for lipid release (I.e. that Q_ϕ should approach $214\ \mathrm{M}^{-3}$) implies that a similar amount of lipid should be released from a complex solution (characterized by a particular Q_ϕ, $[\mathrm{mbCD}]_{\mathrm{total}}$, and temperature) in response to whatever perturbation promoted it to such a state. We investigated this premise (path-independence with respect to lipid release) by monitoring re-nucleation in a single mbCD-POPC mixture from the same instantaneous state, induced by dilution and cooling.

The dilution trajectory that we used in this experiment is labelled as "2." in Figure S3a; data from this experiment are summarized in Figure S3b. To perform this experiment, we first heated an LUV-mbCD mixture to 70 °C to generate a complex solution characterized by $Q_\phi = 800\ \mathrm{M}^{-3}$ and $[\mathrm{mbCD}]_{\mathrm{total}} = 51\ \mathrm{mM}$ (Eq. 6 in the main text) and then cooled the resulting complex solution to 25 °C. The solution was kinetically trapped (see Figure 4a in the main text), granting us a generous window in which to perturb this solution. While holding the solution at 25 °C, we diluted it (along trajectory "2." In Figure S3a) and observed re-nucleation (reflected by an increase in light scattering signal). Again, we heated this mixture to 70 °C to re-complex all lipid. We cooled the solution to 25 °C and observed re-nucleation induced, this time, by cooling. Finally, we heated the mixture to 70 °C once again. In Figure S3b, the two red dots mark the same instantaneous state characterized by $Q_\phi = 1990\ \mathrm{M}^{-3}$ and $[\mathrm{mbCD}]_{\mathrm{total}} = 38\ \mathrm{mM}$ (Eq. 6) from which rapid re-nucleation occurred in response to both perturbations. Immediately after dilution, there was a sharp increase in the amount of scattered light followed by a slow, steady increase; in contrast, the signal plateaued within 15 minutes after cooling. Notably, the normalized intensity one minute after dilution was approximately equal to the plateau after cooling (0.18). This suggests that dilution rapidly nucleated a similar amount of nascent lipid particles (assembled from an equivalent amount of de-complexed lipid from cooling) that slowly condensed into particles of different lamellarities/aggregation states[2] (resulting in more scattered light)[8].

Practically, the above experiment implies that it is valid to predict the re-nucleation behavior of diluted complex solutions by extending observations in Figure 4a in the main text (which were determined via cooling).

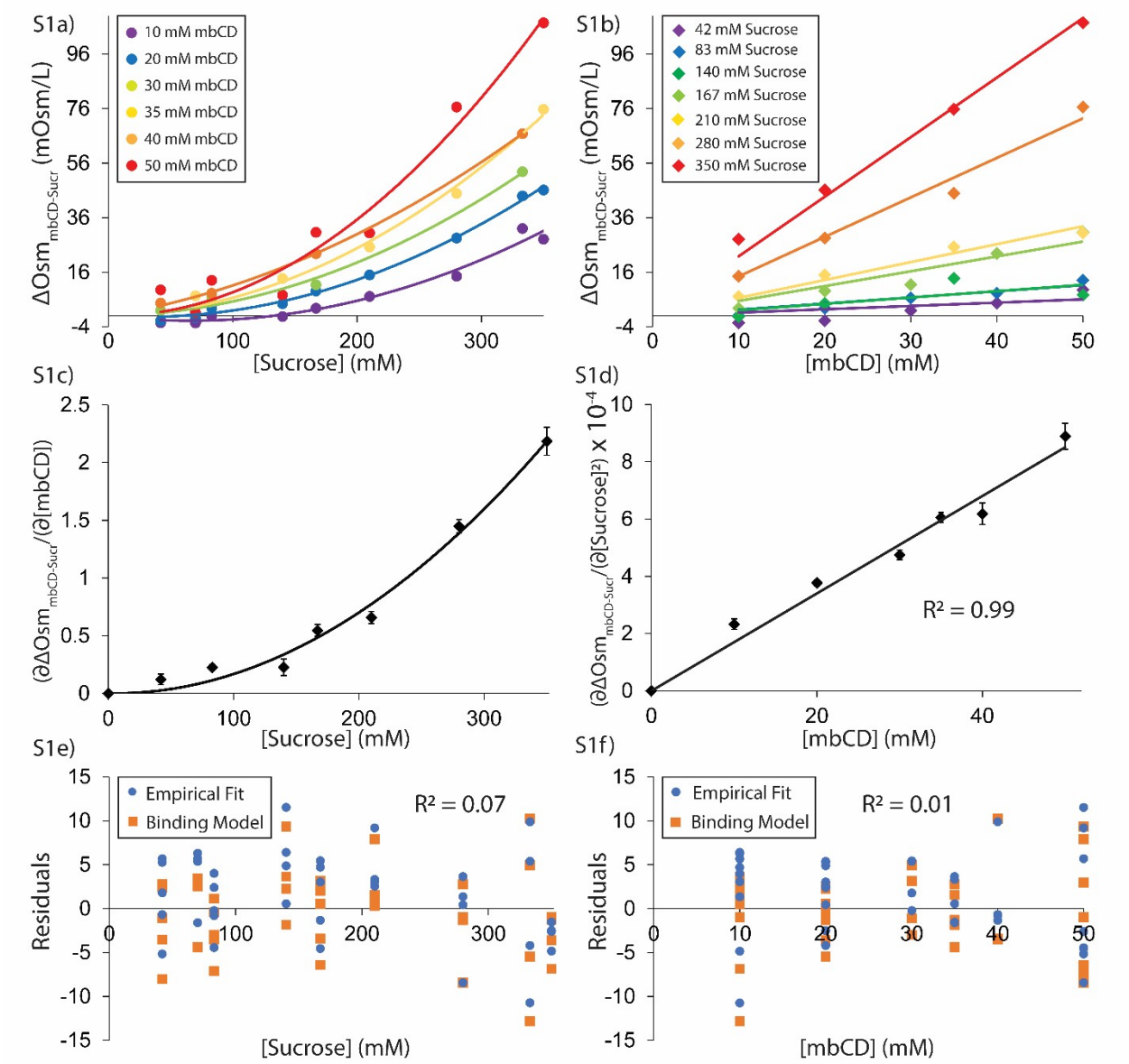

Binary mbCD/Sucrose solutions deviate from ideality. S1a) $^{\Delta Osm_{mbCD\text{ - }Sucr}}$ with respect to $[Sucrose]$ for different series of fixed $[mbCD]$. **S1b)** $^{\Delta Osm_{mbCD\text{ - }Sucr}}$ with respect to $[mbCD]$ for different series of fixed $[Sucrose]$. **S1c)** Partial derivatives of $^{\Delta Osm_{mbCD\text{ - }Sucr}}$ with respect to $[mbCD]$ with respect to $[Sucrose]$. **S1d)** Partial derivatives of $^{\Delta Osm_{mbCD\text{ - }Sucr}}$ with respect to $[Sucrose]^2$ for different $[mbCD]$. **S1e)** Residuals from fits of data in S1a and S1b to the empirical fit and equilibrium binding model with respect to $[Sucrose]$. **S1f)** Residuals from fits of data in S1a and S1b to the empirical fit and equilibrium binding model with respect to $[mbCD]$. Values of R^2 are indicated only for linear fits.

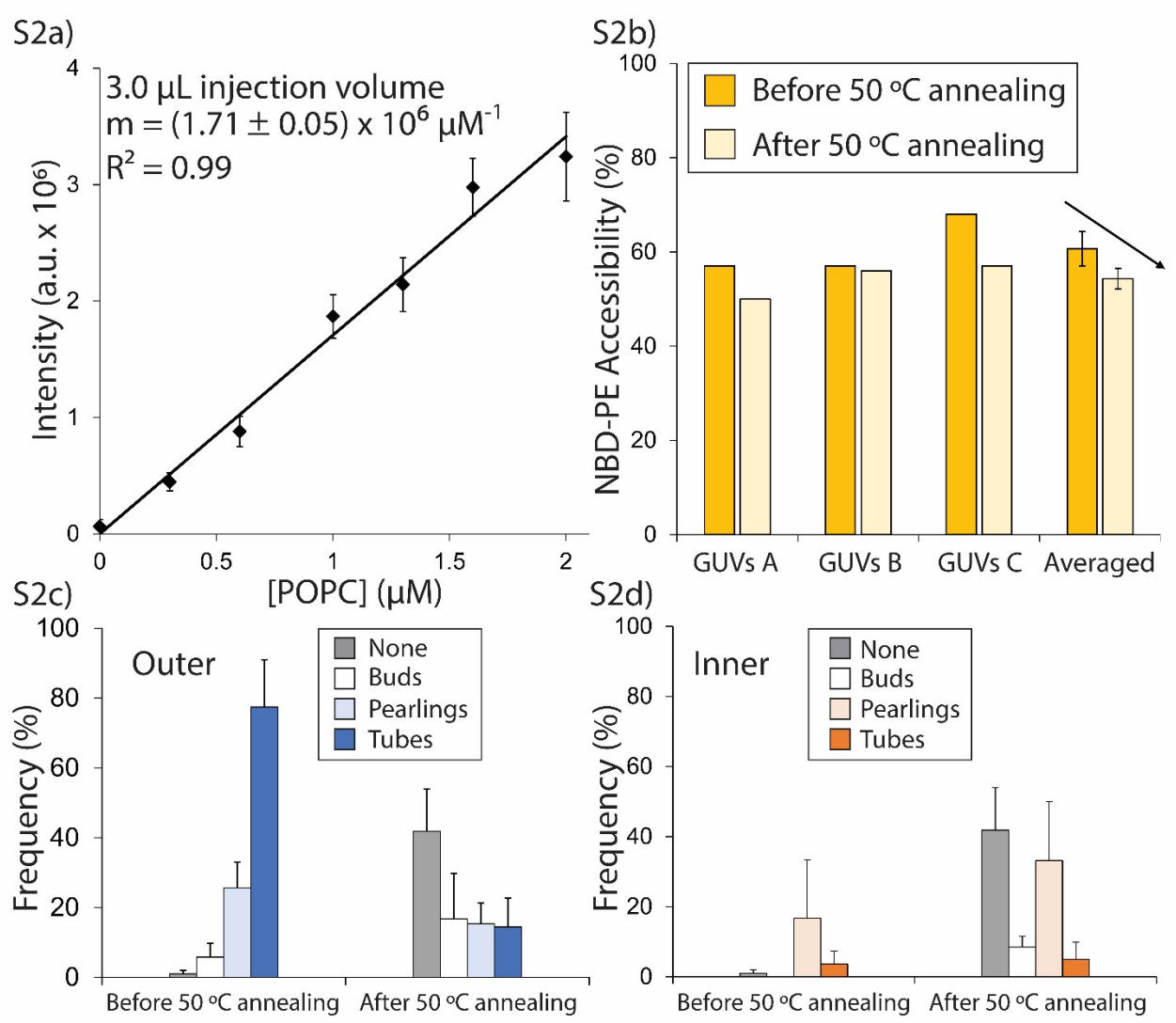

Characterization of GUV dispersions carried into experiments with mbCD. S2a) Standard curve for determination of POPC concentration in GUV dispersions via direct injection onto a mass spectrometer. Error bars are standard errors of the means (SEMs) from three identically-prepared POPC standards. **S2b)** Accessibilities of NBD-PE to sodium dithionite in three separate GUV dispersions before and after 50 °C annealing. The lipid composition of these GUV dispersions were 99.7% POPC//0.3% NBD-PE (mole percentages). Error bars are SEMs from the three GUV dispersions. **S2c)** Types of outer bending protrusions in 99.6% POPC//0.4% Texas Red DHPE (mole fractions) before and after 50 °C annealing. Error bars are SEMs from three GUV dispersions; between 15-40 individual GUVs were observed from each dispersion. **S2d)** Types of inner bending protrusions in 99.6% POPC//0.4% Texas Red DHPE (mole fractions) before and after 50 °C annealing. Error bars are SEMs from three GUV dispersions; between 15-40 individual GUVs were observed from each dispersion. For explanations of the morphologies and collection of these statistics, see the main text.

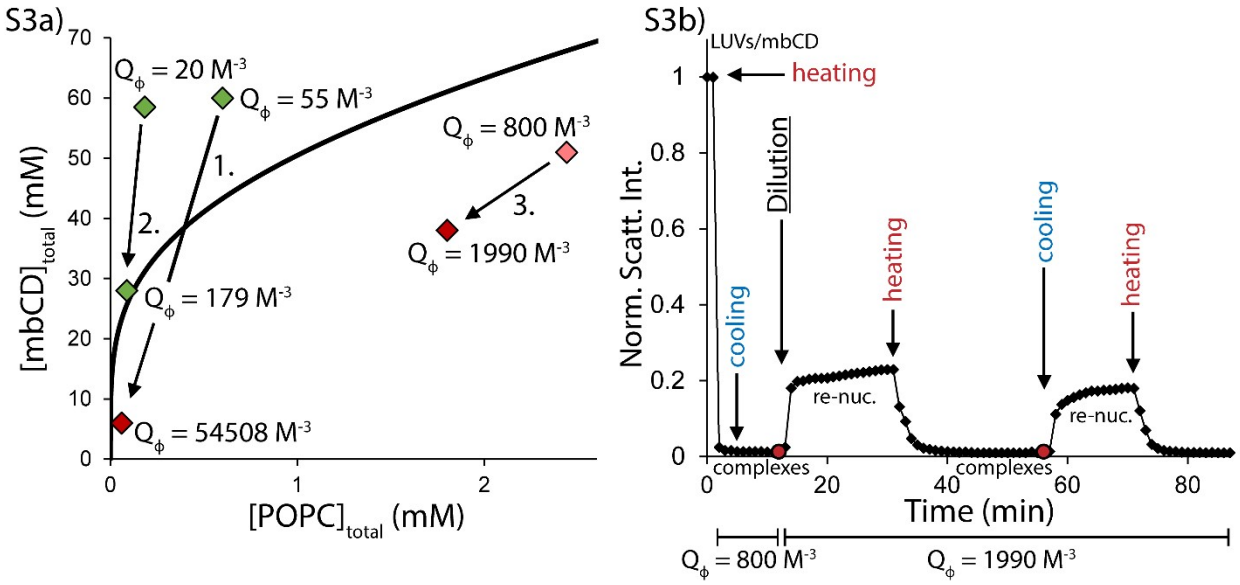

S3a) Pairs of mbCD-lipid mixtures (and dilution-trajectories connecting them) mapped on the RT mbCD-POPC phase diagram (see text for details). Colors match those in Figure 4a in the main text. Trajectory 1 is from a previous publication so the datapoints are absent from Figure 4a. **S3b)** Re-nucleation (re-nuc.) due to dilution at 25 °C and then cooling to 25 °C from 70 °C for the same mixture (see text); dilution followed trajectory 2. from Figure S3a. The experiment began with a mixture of LUVs/mbCD that was promoted to the solubilization region (I.e. complexes) by first heating to 70 °C; all intensities were normalized to that of the initial mbCD-LUV mixture. The dilution-trajectory (trajectory 2. From S3a) was traversed by adding 639 µL of 150 mM Sucrose to 1800 µL of a complex solution of $Q_\phi = 800\ M^{-3}$ with $[mbCD]_{total} = 51\ mM$ at 25 °C. Red dots = instantaneous states of the complex solution characterized by $Q_\phi = 1990\ M^{-3}$ and $[mbCD]_{total} = 38\ mM$ at 25 °C (see text).

Table S1: Mass Spectroscopic Measurements of POPC GUV Suspensions Diluted 1:50 (v:v) in Methanol						
Suspension #	760 m/z	761 m/z	(760+761) m/z	Avg.	Std. Dev.	$[POPC]_{GUVs}$ (μM)
GUVs 01	8.37E+04	2.21E+06	2.30E+06	1.54E+06	6.02E+05	45
		9.07E+05	9.07E+05			
	1.98E+04	1.22E+06	1.24E+06			
	1.33E+04	1.70E+06	1.71E+06			
GUVs 02	6.66E+04	1.69E+06	1.76E+06	1.29E+06	4.30E+05	38
	1.73E+04	1.08E+06	1.10E+06			
		7.94E+05	7.94E+05			
	2.10E+04	1.49E+06	1.51E+06			
GUVs 03	1.04E+05	9.24E+05	1.03E+06	1.01E+06	3.53E+05	30
		5.33E+05	5.33E+05			
	2.64E+04	1.08E+06	1.10E+06			
	1.87E+05	1.19E+06	1.38E+06			
GUVs 04	1.10E+05	3.22E+06	3.33E+06	2.16E+06	8.69E+05	63
	5.96E+04	1.18E+06	1.24E+06			
	3.84E+04	2.01E+06	2.05E+06			
	9.23E+04	1.91E+06	2.01E+06			
GUVs 05	9.27E+04	1.42E+06	1.52E+06	1.79E+06	3.80E+05	52
	1.78E+05	1.48E+06	1.66E+06			
		1.64E+06	1.64E+06			
	1.06E+04	2.35E+06	2.36E+06			
GUVs 06		8.39E+05	8.39E+05	8.49E+05	2.38E+05	25
	7.64E+03	5.90E+05	5.98E+05			
		7.87E+05	7.87E+05			
	1.66E+04	1.15E+06	1.17E+06			
GUVs 07		1.05E+06	1.05E+06	9.88E+05	1.42E+05	29
	2.52E+04	9.24E+05	9.49E+05			
		8.11E+05	8.11E+05			
		1.15E+06	1.15E+06			
GUVs 08	7.98E+03	1.37E+06	1.38E+06	1.48E+06	2.93E+05	43
	2.10E+03	1.46E+06	1.47E+06			
	1.09E+05	1.07E+06	1.18E+06			
		1.88E+06	1.88E+06			
GUVs 09	1.12E+05	1.49E+06	1.60E+06	1.53E+06	1.73E+05	45
	2.32E+04	1.62E+06	1.64E+06			
		1.60E+06	1.60E+06			
	8.06E+04	1.19E+06	1.27E+06			
GUVs 10	1.48E+04	9.09E+05	9.24E+05	2.24E+06	1.09E+06	66
		3.17E+06	3.17E+06			
		1.76E+06	1.76E+06			
		3.12E+06	3.12E+06			
GUVs 11		1.37E+06	1.37E+06	1.78E+06	3.89E+05	52
	2.22E+04	1.51E+06	1.54E+06			
	2.02E+04	2.18E+06	2.20E+06			
	1.45E+04	1.99E+06	2.00E+06			
					Avg. (μM) =	44
					SEM (μM) =	4

1. Anderson TG, Tan A, Ganz P, Seelig J. Calorimetric measurement of phospholipid interaction with methyl-beta-cyclodextrin. BIOCHEMISTRY. 2004;43(8):2251-61. doi: 10.1021/bi0358869. PubMed PMID: WOS:000189185700012.

2. Bozelli JC, Hou YH, Epand RM. Thermodynamics of Methyl-beta-cyclodextrin-Induced Lipid Vesicle Solubilization: Effect of Lipid Headgroup and Backbone. LANGMUIR. 2017;33(48):13882-91. doi: 10.1021/acs.langmuir.7b03447. PubMed PMID: WOS:000416877600021.
3. Huang Z, London E. Effect of Cyclodextrin and Membrane Lipid Structure upon Cyclodextrin-Lipid Interaction. LANGMUIR. 2013;29(47):14631-8. doi: 10.1021/la4031427. PubMed PMID: WOS:000327360500036.
4. Steinkuhler J, De Tillieux P, Knorr RL, Lipowsky R, Dimova R. Charged giant unilamellar vesicles prepared by electroformation exhibit nanotubes and transbilayer lipid asymmetry. SCIENTIFIC REPORTS. 2018;8. doi: 10.1038/s41598-018-30286-z. PubMed PMID: WOS:000440977900003.
5. Dobereiner HG, Evans E, Kraus M, Seifert U, Wortis M. Mapping vesicle shapes into the phase diagram: A comparison of experiment and theory. PHYSICAL REVIEW E. 1997;55(4):4458-74. doi: 10.1103/PhysRevE.55.4458. PubMed PMID: WOS:A1997WV24900084.
6. Svetina S, Zeks B. Shape behavior of lipid vesicles as the basis of some cellular processes. ANATOMICAL RECORD. 2002;268(3):215-25. doi: 10.1002/ar.10156. PubMed PMID: WOS:000178870800007.
7. Allhusen JS, Conboy JC. The Ins and Outs of Lipid Flip-Flop. ACCOUNTS OF CHEMICAL RESEARCH. 2017;50(1):58-65. doi: 10.1021/acs.accounts.6b00435. PubMed PMID: WOS:000392457800008.
8. Pencer J, Hallett FR. Effects of vesicle size and shape on static and dynamic light scattering measurements. LANGMUIR. 2003;19(18):7488-97. doi: 10.1021/la0345439. PubMed PMID: WOS:000185086500052.